INL/CON-20-58872-Revision-0

An Overview of Neutron Irradiated SiC Layer Behavior using Micro-and Nano-Characterization Techniques

June 2020

Isabella J Van Rooyen, Subhashish Meher, Karen E Wright, Thomas M Lillo

Changing the World's Energy Future

INL is a U.S. Department of Energy National Laboratory operated by Battelle Energy Alliance, LLC

INL/CON-20-58872-Revision-0

An Overview of Neutron Irradiated SiC Layer Behavior using Micro-and Nano-Characterization Techniques

Isabella J Van Rooyen, Subhashish Meher, Karen E Wright, Thomas M Lillo

June 2020

Idaho National Laboratory
Idaho Falls, Idaho 83415

http://www.inl.gov

Prepared for the
U.S. Department of Energy
Under DOE Idaho Operations Office
Contract DE-AC07-05ID14517

Proceedings of HTR 2020
Yogyakarta, Indonesia, October 6-8, 2020
Paper HTR 2020

An Overview of Neutron-Irradiated SiC Layer Behavior Using Micro- and Nano-Characterization Techniques

Isabella J. van Rooyen[1], S. Meher[2], Karen Wright[3], Thomas Lillo[2]

[1]*Fuel Design and Development Department, Idaho National Laboratory, Idaho Falls, ID 83415, USA*
[2]*Materials Science and Engineering Department, Idaho National Laboratory, Idaho Falls, ID 83415, USA*
[3]*Post-Irradiation Examination Department, Idaho National Laboratory, Idaho Falls, ID 83415, USA*

Abstract – *The complexity of fission product distribution and composition within the SiC layer of tri-structural isotropic (TRISO)-coated particles, along with irradiation effects on the SiC structure in addition to the variable nature of metallic fission product release, resulted in the exploration of various micro- and nano-characterization techniques. The fine scale of fission product precipitates necessitates unique knowledge and application of electron microscopic techniques for irradiated fuel during analysis of the Advanced Gas Reactor (AGR)-1 experiment. A summarized discussion on specific advanced techniques, along with associated method development for TRISO-coated particles is provided, followed by the down-selected techniques currently considered to provide the highest impact. The techniques considered are electron probe microanalysis (EPMA), scanning transmission electron microscopy (STEM), and precession electron diffraction (PED). SiC grain boundary characteristics are evaluated due to the mobility of specific fission products through the grain boundaries. PED was performed to elucidate the role of grain boundary character in fission product transport. One set of comparative analyses of AGR-1 and AGR-2 particles shows that the AGR-1 high-Ag-retention particle had statistically more coincidence site lattice (CSL)-related grain boundaries (but fewer low-angle grain boundaries) compared to the AGR-2 particle. This implies that CSL-related grain boundaries may directly influence Ag retention. However, precipitates were found on a relatively small fraction of CSL-related grain boundaries in both particles. Another set of analyses comparing safety-tested AGR-1 and AGR-2 particles showed significant differences in average SiC grain boundary distributions, though the fission product distributions in these grain boundaries are very similar.*

I. INTRODUCTION

The release of metallic fission products from neutron-irradiated tri-structural isotropic (TRISO) particle fuel designed for advanced high-temperature nuclear reactors has been regularly observed [1,2]. The silicon carbide (SiC) layer TRISO particle acts as the primary barrier for containment of fission products. Advanced nanoscale investigation of TRISO particles, especially the SiC layer, reveals that the fission products react with SiC to form precipitates of various compositions and sizes at the grain boundaries [3,4]. The transport mechanism of silver (^{110m}Ag) has been of interest to the TRISO community, as the release of ^{110m}Ag is a potential worker safety concern due to plate-out on the cooler metallic parts of the helium pressure boundary. In addition, specific fission products such as palladium (Pd) can diffuse through both grain boundaries and in the bulk SiC, forming precipitates at the grain boundaries, as well as forming heterogeneously at structural defects in the bulk SiC [5,6].

Electron microscopic examination of TRISO-coated particles as part of the Advanced Gas Reactor (AGR)-1 and AGR-2 programs was performed [3,4,7] to identify fission product precipitates along the grain boundaries of the SiC layer. The AGR-1 nuclear fuel particles were fabricated at Oak Ridge National Laboratory using 350-µm-diameter mixed uranium-oxide/uranium-carbide (UCO) kernels.

Details on the fabrication methods can be found in [8]. The UCO fuel kernels were fabricated by BWX Technologies as part of the AGR-2 program. The UCO kernels had a mean diameter of 427 nm and a ^{235}U enrichment of 14.0%. The kernels were coated at BWX Technologies in a 150-mm engineering-scale coater, representing an important step toward the establishment of an industrial-scale fuel fabrication capability for the AGR program. The average diameter of the coated UCO particles was 873 nm. The AGR-2 experiment was irradiated in the Advanced Test Reactor at Idaho National Laboratory and contained six independently controlled and monitored capsules. [9].

This paper discusses fission product transport in the SiC layer of TRISO particles from AGR-1 and AGR-2. It provides an overview of the electron microscopy and micro-analytical activities performed at Idaho National Laboratory as part of AGR-1 and AGR-2 post-irradiation examination. Selected results from electron probe microanalysis (EPMA), transmission electron microscopy (TEM), and precession electron diffraction (PED) on inter- and intragranular fission product distribution in SiC are also discussed.

II. EXPERIMENT, SAMPLE DESCRIPTION, AND CHARACTERIZATION METHODS

II.A. Particle Selection and Irradiation Conditions

For a comparative study of AGR-1 and AGR-2, high-Ag-retention fuel particle AGR1-632-034, was compared with a low-Ag-retention AGR2-222-RS036 fuel particle. In the baseline TRISO particles, the kernels were coated, via fluidized-bed chemical vapor deposition, with a porous buffer layer (≈100 μm), a dense inner pyrolytic carbon (IPyC) layer (≈40 μm), a silicon carbide (SiC) structural containment layer (≈35 μm), and a dense outer pyrolytic carbon (OPyC) layer (≈40 μm). In the AGR-2 program, the fabrication parameters for applying TRISO coatings to both types of kernels were based on those used earlier for the AGR-1 Variant 3 fuel. In Variant 3-type fuel, the SiC layer was deposited at lower temperatures in an argon-hydrogen mixture. This produced a finer grain structure and was expected to reduce SiC defects caused by uranium dispersion [9].

The microscopic analyses of two safety-tested particles, AGR1-433-001 and AGR2-223-RS006, are also compared in this study. Details on the irradiation conditions of these particles are given in Table 1. Figure 1 shows a schematic of the characterization tools used in this program to better understand the micro- and nanoscale behavior of neutron irradiated TRISO particles.

Table 1: TRISO particle characteristics and average compact irradiation conditions (PS: pilot scale, BDL: below detection level, FIMA: fissions per initial metal atom, TAVA: temperature average volume average) [10,11].

Compact	Fuel Type	Ag Retention (%)*	Burnup (%FIMA) #	Fast Neutron Fluence (10^{25} n/m^2)	TAVA Temp. (°C)	Time-Avg Peak Temp (°C)
AGR1-632-034	Baseline	65	11.4	2.55	1070	1144
AGR1-433-001 (Safety-tested)	Variant 3	39	18.6	4.16	1094	1179
AGR2-222-RS036 (Safety-tested)	PS Variant 3	BDL	12.6	3.39	1287	1354
AGR2-223-RS006	PS Variant 3	8	12.7	3.46	1296	1360
AGR2-222-RS019	PS Variant 3	20	12.55	3.39	1287	1354

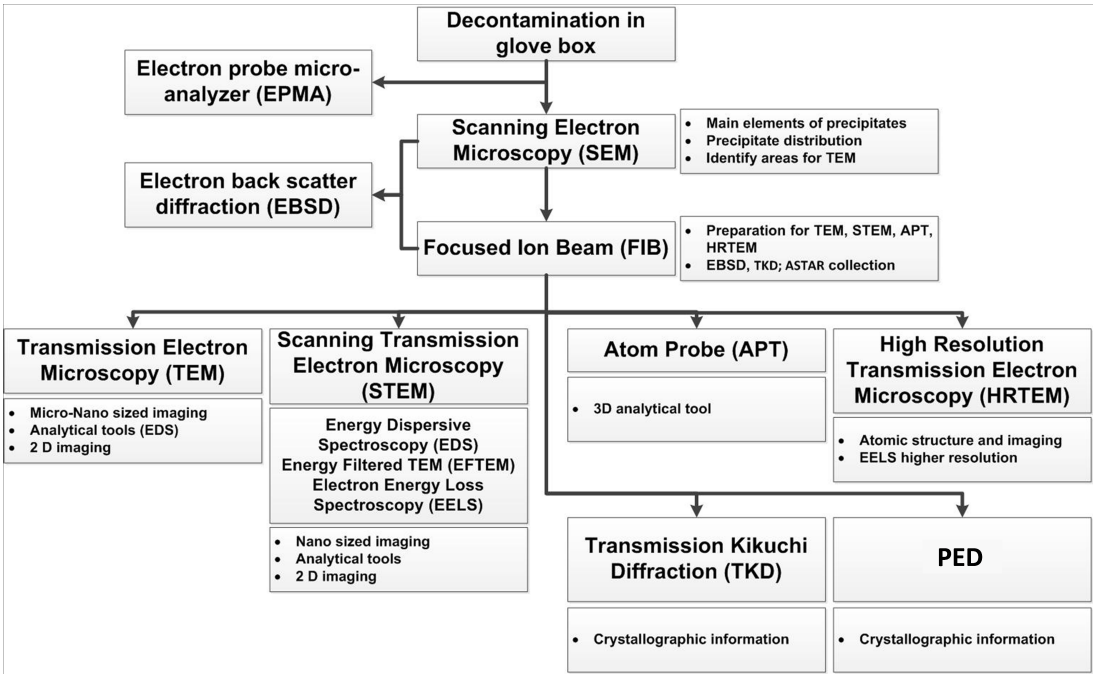

Fig. 1: Overview of the characterization methods utilized for understanding fission product transport behavior in neutron irradiated TRISO particles.

III. RESULTS AND DISCUSSION

A comprehensive description of the AGR-1 advanced microscopy program is detailed elsewhere [12]. The results in this paper focus on selected AGR-2 data and their relationship to AGR-1 data, specifically addressing fission product distribution in the SiC layer of AGR-1 and AGR-2 particles, with a particular focus on (a) accurate quantification of elemental composition, (b) accurate segregation of elements in precipitates, (c) the relationship in both grain boundary nature and fission-product precipitates, (d) and transport mechanisms throughout the intact layers (specifically for Ag and Pd).

III.A. Electron Probe Microanalyses of AGR-1 and AGR-2 Safety-Tested Particles

EPMA is an electron beam technique like scanning electron microscopy; but whereas the latter is optimized for image collection, EPMA is optimized for quantitative chemical analysis on a micrometer spatial scale. For several decades, electron probe microanalysis has been used for fission product quantification in irradiated nuclear fuels, due to its ability to detect fission products as small as ~100 ppm. For the AGR-1 and AGR-2 programs, EPMA was used to measure the distribution of approximately 20 fission products across numerous particles—both irradiated and safety-tested. In this example, EPMA tracked the fission product distribution across two radii on two different safety-tested particles—one each from the AGR-1 and AGR-2 experiments. The first particle, AGR1-433-003, was irradiated to 18.6% FIMA with a TAVA of 1094°C, while the second particle, AGR2-222-RS19, was irradiated to 12.55% FIMA with a TAVA of 1287°C. Both particles retained < 20% of ^{110m}Ag.

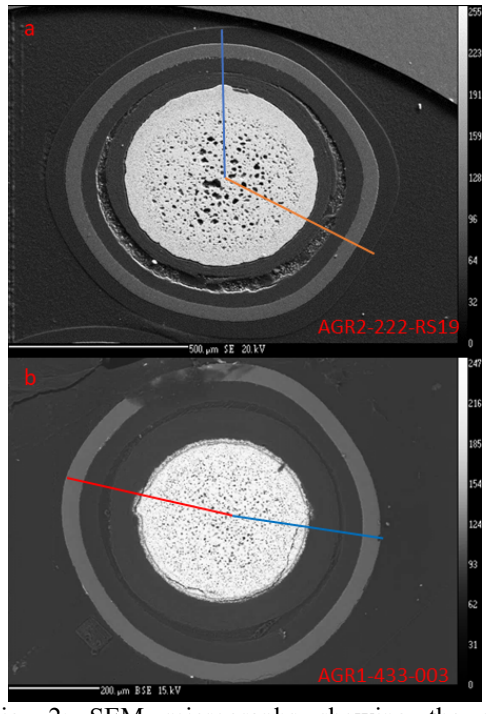

Fig. 2: SEM micrographs showing the profile projections from particles (a) AGR2-222_RS06 and (b) AGR1-433-003, with orange lines at the gap side and blue lines at the non-gap side.

Figure 3 (a-b) shows the Cs profile across both particles. Though these particles differ in several ways (burnup, TAVA, fabrication method), the Cs distribution across these particles is quite similar.

Both particles show similar quantities of Cs retained in the kernel, as well as similar quantities present in the IPyC. The largest significant difference is the fact that, for particle AGR2-222-RS19, Cs penetrates the SiC layer on the side of the particle lacking a gap between the buffer and IPyC (Figure 4).

Figure 3 (c-d) shows the Pd profile across both particles. This profile is particularly useful, as it is an easier-to-detect surrogate for Ag distribution. As with Cs, the Pd distribution profile is quite similar between the two specimens, with the most significant difference being a large concentration of Pd at the SiC-IPyC interface of AGR2-222-RS19 on the non-gap side.

Because fission product release from particles is of concern, it is useful to determine how far into the outer particle layers key fission products penetrate. Since EPMA typically has a detection limit of approximately 100 ppm for many fission products, Figure 3 shows select elements present at levels greater than 100 ppm in the outer particle layers. In both particles, Pd penetrates the SiC layer on at least one measured radius. Cs penetration is significantly greater in particle AGR2-222-RS19, nearly penetrating through the OPyC on the non-gap side; while in particle AGR1-433-003, it penetrates about 4 mm into the SiC layer. For both particles, Ag penetration is not detected beyond the SiC-IPyC interface.

While many fission products are rather symmetrically distributed across the particle, some are not. Figure 5 shows the Sr distribution across the measured radii of both particles. In both the AGR-1 and AGR-2 particles, peak Sr concentration occurs in the kernel periphery—the kernel's outermost perimeter—which is particularly carbon-rich. Moreover, Sr distribution is typically asymmetrical, with its apex on the hypothesized cooler side of the particle. This behavior is emulated by Ba, Te, and sometimes Eu. These data show how EPMA can elucidate fission product distribution in irradiation TRISO particles, and it demonstrates similarities in the behavior of AGR-1 and AGR-2 safety-tested particles. This could be a consequence of the effects of safety testing overwhelming the irradiation effects; however, AGR1 and AGR2 irradiated particles (but not safety tested) also exhibit similar fission product distribution behaviors prior to safety testing.

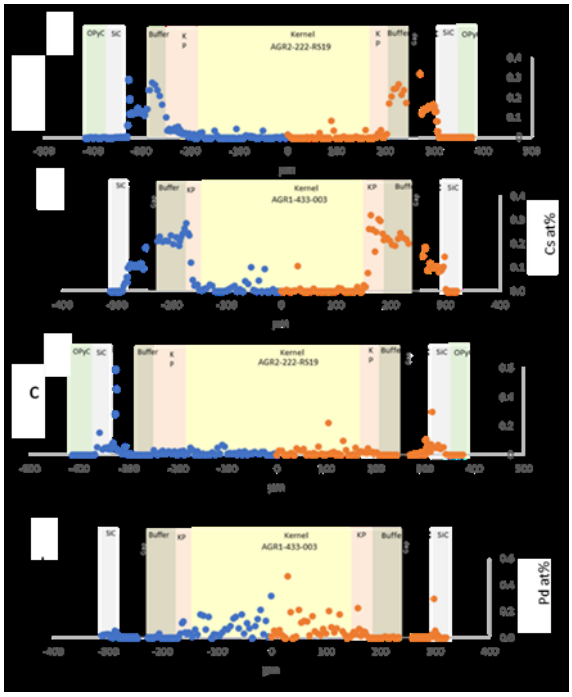

Fig. 3: Cs profile across the two radii in particles AGR2-222-RS19 and AGR1-433-003 (a-b); Pd profile across the two radii in particles AGR2-222-RS19 and AGR1-433-003 (c-d). Orange symbols represent a radius with an aberration such as a kernel bulge or a large gap between the buffer and IPyC, while blue symbols represent a radius with fewer imperfections.

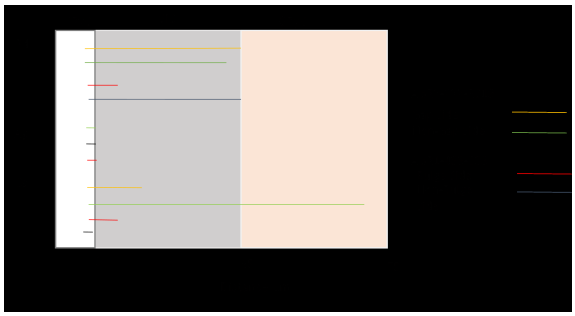

Fig. 4: Penetration depth of Pd, Ag, and Cs into the outer layers of both particles. Note that fission product quantity in the OPyC was not measured in particle AGR1-433-003.

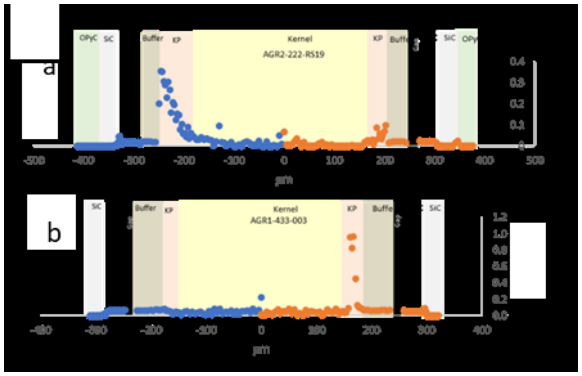

Fig. 5: (a-b) Sr profile across the two radii in

particles AGR2-222-RS19 and AGR1-433-003. Orange symbols represent a radius with an aberration such as a kernel bulge or a large gap between the buffer and IPyC, while blue symbols represent a radii with fewer imperfections.

III.B. TEM Results of Chemical Analysis

TEM samples were prepared using a dual-beam Quanta 3D focused ion beam instrument. To minimize potential Ga ion damage, the samples were cleaned using a voltage of 5 kV and current of ~50 pA for 2–5 minutes per side. Scanning transmission electron microscopy and conventional TEM imaging were conducted on a FEI Tecnai F30 microscope operated at 300 kV. Chemical analyses of the TEM samples were carried out using the EDAX energy-dispersive spectroscopy (EDS) system. Gatan Digital Micrograph and TEM imaging and analysis software were used for post-processing of the TEM data.

In this study, two particles (AGR1-632-034 and AGR2-223-RS006), with similar burnup but different fabrication methods and Ag retention are compared. Also, microscopic results from two safety-tested (at 1600°C) particles from the AGR-1 and AGR-2 experiments are compared.

Identification of Ag in Grain Boundaries and Triple Points

Figure 6 (a-b) shows the presence of Ag as a fission product in the SiC grain boundaries in both the AGR-1 and AGR-2 particles. Figure 6 (b) shows the presence of Ag in the triple junction itself (marked "2") in the SiC layer near the edge of the IPyC. EDS data corresponding to Figure 6 (a) can be found elsewhere [4], while EDS data corresponding to Figure 6 (b) is provided in Table 2. In Table 2, it is observed that the Ag transport is also potentially accompanied by a small amount of Cd.

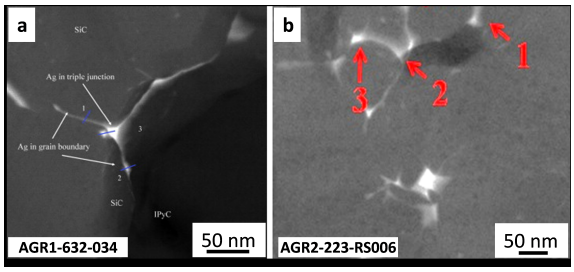

Fig. 6: STEM images identify Ag in SiC grain boundaries and triple junctions in (a) AGR-1 [4] and (b) AGR-2 TRISO particles.

Table 2. Qualitative spot EDS compositions from the locations highlighted in Figure 5 (b) taken from particle AGR2-223-RS006.

Point	Si	C	Pd	Ag	Cd	U
1	55.9	41.1	0.46	**2.45**	0.01	0
2	54.8	40.8	0	**3.56**	0.75	0.05
3	52.7	41.4	0.17	**5.08**	0.67	0

Identification of Pd both Inter- and Intragranularly in SiC

It was recently discovered that precipitation of intragranular Pd containing fission products in the SiC layer of neutron-irradiated TRISO particles possibly occurs via a novel, dual-step nucleation mechanism [6,13]. In the first step, β-SiC is transformed into a nanoscale α-SiC phase, mostly nucleated at heterogeneous nucleation sites such as stacking faults. Then, Pd reacts with the Si in the α-SiC to form Pd silicide and it imprints into the morphological templates of α-SiC precipitates. Such unique Pd transport within the β-SiC was reported in the TRISO particles of both the AGR-1 and AGR-2 experiments [6].

For example, Figure 7 (a) shows an AGR-1 STEM image in which fully transformed Pd silicide and semi-transformed Pd precipitate on an α-SiC template can be observed. Details on chemical analyses of these regions by EDS are provided in Table 3, confirming the presence of Pd. Recently, the physical understanding of intragranular fission product precipitation has been enhanced through both advanced microscopy and first-principle calculations [5,14,15].

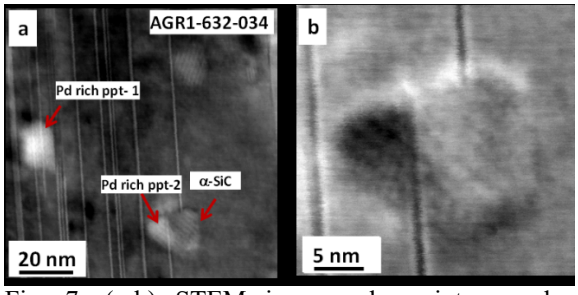

Fig. 7: (a-b) STEM images show intragranular transport of Pd in the SiC layer of TRISO particles, occurring via a dual-step transformation process.

Table 3. Qualitative spot EDS compositions from the locations highlighted in Figure 6.

	Si	C	Pd	Ag	Cd	U
Pd-rich ppt-1	66.9	29.4	0.7	**0**	0.2	0.1
Pd-rich ppt-2	66.5	29.4	0.8	**0**	0	0
α-SiC	62.1	37.0	0.2	**0**	0	0

Qualitative Chemical Composition of Fission Product Precipitates Using EDS

Conventionally, large-scale precipitates in TRISO fuels are assumed to be complex compounds of fission products. The STEM image in Figure 8 (a) shows precipitates in the SiC layer of particle AGR2-222-RS036. Figure 8 (b), with high spectral and spatial resolution, reveals the different segregation behavior of fission products within a single precipitate. Preliminary results reveal that Mo and Pd segregate to different regions of the same precipitate in SiC, while U is almost uniformly distributed. These results clearly indicate that fission products segregate within the precipitates in TRISO fuels, and the chemical affinity or bonding between them is not equally favorable to the formation of a compositionally homogeneous precipitate. Rather, fission products strongly segregate within the precipitates to form segregated regions that impart the mass contrast in the STEM images. However, it is not yet clear whether this is equilibrium segregation or metastable chemical segregation due to cooling from a high temperature. Similar segregation is also observed in the IPyC layer of the AGR1-523-SP01 particle [5].

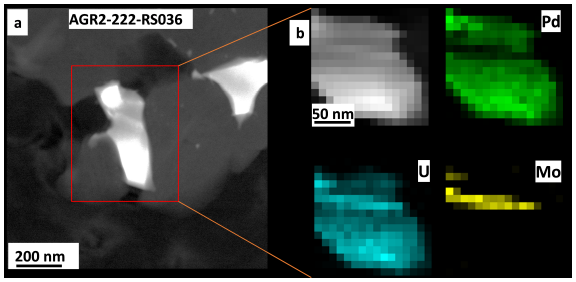

Fig.8: (a) STEM image showing grain boundary fission product precipitates, and (b) associated fission-product spatial maps showing the different chemical segregations within the same large precipitate in the SiC layer of TRISO particle AGR2-222-RS036.

III.C. SiC Grain Boundary Nature and Their Association with Fission Products Using PED

Figure 9 (a) shows comparative SiC grain boundary analyses of AGR-1 and AGR-2 particles with similar fuel burnup levels but different fabrication methods and Ag retention. Table 1 shows AGR1-632-034 as a baseline fuel with high Ag retention (65%), while AGR2-223-RS006 is a Variant 3-type fuel with low Ag retention (8%). Grain boundary information was collected using PED, and crystallographic information was exported and analyzed using EDAX OIM v7.1.0 software. Figure 9 (a) shows that the high-Ag-retention AGR-1 particle had statistically more CSL-related grain boundaries (but fewer low-angle grain boundaries) than the AGR-2 particle. This implies that CSL-related grain boundaries may directly influence Ag retention. However, Figure 9 (b) shows that, in both particles, precipitates were found in a relatively small fraction of CSL-related grain boundaries. Fission product precipitates were found in low-angle grain boundaries of the AGR-1 particle only.

Similarly, Figure 10 plots a comparative grain boundary analysis of safety-tested (at 1600°C) and Variant 3 AGR-1 and AGR-2 particles. In Table 1, Ag retention in AGR1-433-001 and AGR2-222-RS036 is 39% and below the detection limit, respectively. In Figure 10 (a), the AGR-2 particle appears to have a significantly higher percentage of high-angle and CSL grain boundaries. As high-angle and CSL grain boundaries facilitate the majority of fission product precipitation in SiC, the AGR-2 particle may contain a larger amount fission product at grain boundary compared to the AGR-1 particle. Figure 10 (b) shows that these safety-tested particles have a similar fraction of precipitates in each type of grain boundary, despite their different grain boundary distributions.

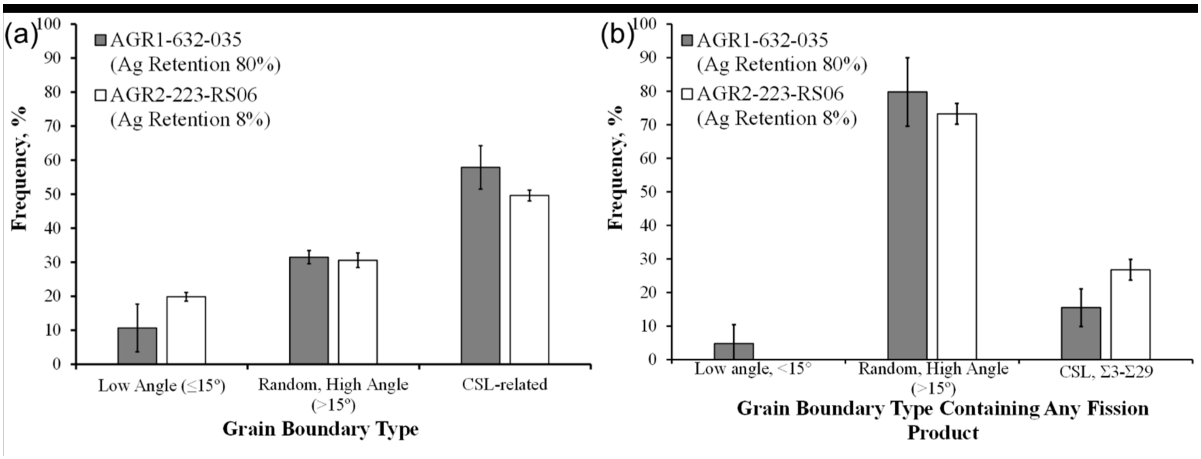

Fig. 9: Comparison of SiC grain boundary types in AGR-1/AGR-2 irradiated TRISO particles, showing the effect of fabrication methods on grain boundaries and fission product transport in particles with near-identical burnup levels.

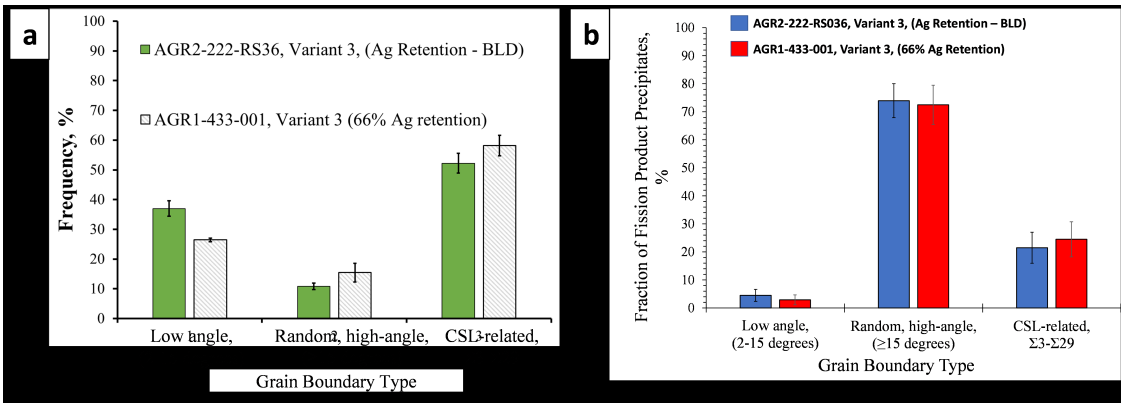

Fig. 10: Comparison of SiC grain boundary types in AGR-1/AGR-2 irradiated and safety-tested TRISO particles.

IV. CONCLUSIONS

Comparative AGR-1 and AGR-2 post-irradiation advanced microscopy and micro-analytical examination provided substantive new information on fission product behavior, summarized as follows:

EPMA results suggest that Cs penetration is significantly greater in particle AGR2-222-RS19, penetrating nearly through the OPyC on the non-gap side; while in particle AGR1-433-003, it penetrates up to 4 mm into the SiC layer.

EPMA results also suggest that Ag penetration is not detected beyond the SiC-IPyC interface in both AGR-1 and AGR-2 particles investigated.

Based on the TEM results, Ag is identified at intergranular sites within the SiC layer in both the AGR-1 and AGR-2 particles. The Ag is usually accompanied by Cd and a small amount of Pd.

The fission product Pd can transport inter- and intragranularly in the SiC layer. However, intragranular transport of Pd is accomplished through a dual-step nucleation process requiring polymorphic transformation of β-SiC into α-SiC.

Large-scale fission product precipitate composition in the SiC layer is not homogeneous in nature. Compositional segregation within precipitates in the SiC layer demonstrates that Mo and Pd are segregated within the same precipitate.

In a comparative study of AGR1-632-034 and AGR2-223-RS006 particles with similar burnup levels but different burnup levels and Ag retention, fission product precipitates are found in low-angle grain boundaries of the AGR-1 particle only, while the AGR-2 particle has a higher fraction of precipitates in CSL grain boundaries as compared to the AGR-1 particle. In a similar comparison of safety-tested AGR1-433-001 and AGR2-222-RS036 particles, there are significant differences in the average SiC grain boundary distributions, but the fission product distributions for these grain boundaries are very similar.

ACKNOWLEDGEMENT

This work was sponsored by the U.S. Department of Energy, Office of Nuclear Energy, under U.S. Department of Energy Idaho Operations Office Contract DE-AC07-05ID14517, as part of the ART Program. The United States Government retains and the publisher, by accepting the article for publication, acknowledges that the U.S. Government retains a nonexclusive, paid-up, irrevocable, worldwide license to publish or reproduce the published form of this manuscript, or allow others to do so, for U.S. Government purposes. The authors wish to acknowledge the efforts of Dr. Daniel Murray and Dr. Fei Teng regarding focused ion beam fabrication of the transmission electron microscope samples, as well as other staff at the Materials and Fuels Complex at Idaho National Laboratory. Transmission electron microscopy work was carried out at the Center for Advanced Energy Studies (CAES)-Microscopy and Characterization Suite (MaCS).

REFERENCES

[1] H. Nabielek, P.E. Brown, P. Offerman, Nucl. Technol., 35 (1977), p. 48.

[2] P.A. Demkowicz et al, Preliminary results of post-irradiation examination of the AGR-1 TRISO fuel compacts, Paper HTR2012-3-021, in: Proceedings of the HTR 2012, Tokyo, Japan, October 28–November 1, 2012.

[3] I.J. van Rooyen, T.M. Lillo, Y.Q. Wu, Journal of Nuclear Materials, 446 (2014) 178-186.

[4] T.M. Lillo, I.J. van Rooyen, Journal of Nuclear Materials, 460 (2015) 97-106.

[5] S. Meher, I.J. van Rooyen, C Jiang, Journal of Nuclear Materials, 527 (2019) 151793.

[6] S. Meher, I.J. van Rooyen, T.M. Lillo, Scientific Reports, 8, (2018) 98.

[7] T.M Lillo, I.J. van Rooyen, S. Meher, Proceedings of HTR (2018), Paper No. 3025.

[8] I.J. van Rooyen, T.M. Lillo, H.M. Wen, C.M. Hill, T.G. Holesinger, Y.Q. Wu, and J.A. Aguiar, Proceedings of HTR (2016).

[9] F.J. Roce, J.D. Stempien, P.A. Demkowicz, Nuclear Design and Engineering, 329, (2018) 73-81.

[10] J.T. Maki, AGR-1 Irradiation Experiment Test Plan, INL/EXT-05-00593 Rev. 3, Idaho National Laboratory (INL) (2009)

[11] B.P. Collin, AGR-2 Irradiation Test Final As-Run Report, INL/EXT-14-32277, rev. 2, August

2014.

[12] I.J. van Rooyen et al., Advanced Electron Microscopy and Micro analytical technique development and application for Irradiated TRISO Coated Particles from the AGR-1 Experiment, INL/EXT--15-36281, 2017.

[13] C. M. Parish, T. Koyanagi, S. Kondo, Y. Katoh, Scientific Reports 7, 1198 (2017).

[14] E. J. Olivier, J. H. Neethling, I. J. van Rooyen, Journal of Nuclear Materials, 532, (2020) 152043.

[15] C. Jiang, S. Meher, I.J. van Rooyen, Computational Materials Science, 171, (2020) 109238.